coatings

MDPI

Article

Investigation on Corrosion Resistance and Formation Mechanism of a P–F–Zr Contained Micro-Arc Oxidation Coating on AZ31B Magnesium Alloy Using an Orthogonal Method

Yuanyuan Zhu [1], Wenhui Chang [1], Shufang Zhang [1], Yingwei Song [2], Huade Huang [1], Rongfang Zhao [1], Guoqiang Li [1], Rongfa Zhang [1,*] and Yijia Zhang [1]

[1] School of Materials and Electromechanics, Jiangxi Science and Technology Normal University, Nanchang 330013, China; 18679934872@163.com (Y.Z.); 13647089261@163.com (W.C.); zhang63793@163.com (S.Z.); hhdtiger@163.com (H.H.); zhaorfamy@126.com (R.Z.); 18435163505@126.com (G.L.); 15941847663@163.com (Y.Z.)

[2] Key Laboratory of Nuclear Materials and Safety Assessment, Institute of Metal Research, Chinese Academy of Sciences, Shenyang 110016, China; ywsong@imr.ac.cn

* Correspondence: rfzhang-10@163.com; Tel./Fax: +86-791-8853-7923

Received: 12 February 2019; Accepted: 13 March 2019; Published: 19 March 2019

Abstract: In this study, the synergistic effects of NH_4HF_2, sodium phytate ($Na_{12}Phy$), K_2ZrF_6, and treatment time on corrosion resistance of a micro-arc oxidation (MAO) treated magnesium alloy and the entrance mechanism of P, F, and Zr into anodic coatings were investigated using an orthogonal method. In addition, the roles of NH_4HF_2, $Na_{12}Phy$, and K_2ZrF_6 on coating development were separately studied. The results show that NH_4HF_2 and $Na_{12}Phy$, the corrosion inhibitors of magnesium alloys, are beneficial but K_2ZrF_6 is harmful to developing anodic coatings. The corrosion resistance of MAO coatings is synergistically determined by coating characteristics, though the coating thickness plays a main role. $Na_{12}Phy$ significantly improves but NH_4HF_2 decreases the corrosion resistance of MAO coatings, while excess high K_2ZrF_6 is harmful to the coating corrosion resistance. Treatment time can increase the coating thickness but is the least important factor in corrosion resistance. During MAO, NH_4HF_2, $Na_{12}Phy$, and K_2ZrF_6 take part in coating formation, causing P, F, and Zr to compete with each other to enter into anodic coatings.

Keywords: magnesium alloy; micro-arc oxidation; corrosion resistance; fluorine; zirconium

1. Introduction

Fractures and bone defects occur frequently due to road traffic accidents and sports injuries [1]. Magnesium alloys appear to be the most promising biomedical metal due to their several advantages over the permanent metallic materials currently in use, including similar density and Young's modulus to human bone, good biocompatibility, and many functions of Mg ions in vivo [2]. However, the major obstacle hampering the clinical applications of magnesium alloys is their rapid degradation in vivo [2,3]. The degradation rate must be controlled before magnesium alloys can be safely used as implants, and therefore the method of surface modification is widely used to limit their deterioration [2,3].

Micro-arc oxidation (MAO), also called plasma electrolytic oxidation (PEO), is one relatively novel and eco-friendly surface modification method that generates porous ceramic-like coatings on light alloys such as magnesium [2,4], aluminum [5], and titanium [6]. The performance of MAO coatings is determined by several factors, including the composition and concentration of selected electrolytes, the applied electrical parameter, and the substrate [2,7–10]. Among these factors, the

electrolyte composition plays an important role in determining the coating performance [3,11–14]. By adopting proper processing factors, MAO can provide hard scratch- and corrosion-resistant coatings on magnesium alloys [3,11–13], thereby effectively improving their biocompatibility [3,13–15].

Potassium fluorozirconate (K_2ZrF_6), a MAO electrolyte containing fluorine (F) and zirconium (Zr) elements, has recently received increasing attention [11,16–21]. Results show that in a solution containing K_2ZrF_6, the developed self-sealing MAO coatings can considerably improve the corrosion resistance of magnesium alloys [17–19]. Zirconium oxide implants are bioinert and have good biocompatibility, high strength, high compression resistance, and excellent wear resistance [22,23]. A particularly compelling find is that zirconia can inhibit bacterial adhesion and colonization on the surface [22,24,25] Fluorine-containing electrolytes such as KF [3,13,14,17,26] and NaF [19,27] can improve the coating corrosion resistance due to enhanced coating thickness, compact microstructure, and a stable MgF_2 product [13,17,26,27]. Moreover, F is an essential trace element in humans, and a proper amount of F can promote bone development [28] and prevent dental caries [29]. The recommended dietary allowance (RDA) for F is 4 mg day^{-1} [30], and high levels of F amount will harm health, such as dental fluorosis [31], denser bones, joint pain, and a limited range of joint movement [32]. In order to fabricate MAO coatings with excellent corrosion resistance and good biocompatibility, investigating the influences of processing factors on corrosion resistance and chemical compositions (especially the F amount of MAO coatings) is required yet rarely reported.

In this study, ammonium hydrogen fluoride (NH_4HF_2), usually used as corrosion inhibitor of magnesium alloys [33,34] but barely as MAO electrolyte on magnesium alloys [32,35], was selected as a fluorine-containing substance and K_2ZrF_6 as the source of both Zr and F to fabricate MAO coating on AZ31B magnesium alloy by MAO process. Sodium phytate (abbreviated as $Na_{12}Phy$), the main form of phosphorus (P) storage in plants, was applied as an environmentally friendly MAO electrolyte on magnesium alloys [12]. Treatment time is a major processing parameter and has significant effect on the thickness [36]. In this study, the main research is presented as follows: (1) the synergetic effect of NH_4HF_2, $Na_{12}Phy$, K_2ZrF_6, and treatment time on the corrosion resistance of MAO coatings was investigated by an orthogonal method; (2) the influences of NH_4HF_2, $Na_{12}Phy$, and K_2ZrF_6 on coating development capability were investigated by observing surface morphology and measuring the I_{corr} values of untreated AZ31B alloy in corresponding solutions; and (3) the entrance mechanisms of P, F, and Zr into MAO coatings were deduced according to the experimental results, electrolyte properties, and MAO characteristics.

2. Experiment

2.1. Materials and Coating Preparation

AZ31B magnesium alloys were machined into the samples with a cuboidal shape of $10 \times 10 \times 6$ mm^3. Prior to MAO treatment, all samples were ground with 80–1000 grit SiC waterproof abrasive paper, cleaned sequentially with tap water followed by distilled water, and then dried with a hair dryer.

As listed in Table 1, the influences of NH_4HF_2, $Na_{12}Phy$, and K_2ZrF_6 concentration, as well as treatment time on corrosion resistance and the amounts of P, F, and Zr in MAO coatings, were investigated by using the orthogonal method of four factors with three levels. According to the processing parameters in Table 1, nine MAO samples designated as Nos. 1–9 were fabricated.

The MAO treatment was carried out by a MAO5D power supply (Chengdu Tongchuang New Material Surface Engineering and Technology Center, Chengdu, China) using a positive pulse constant current control mode. The used electrical parameters were a current density of 50 mA/cm^2, a duty cycle of 35%, and a frequency of 2000 Hz.

Table 1. The orthogonal array and experimental results about the contents of P, F, and Zr elements.

Process	NH_4HF_2 (g/L)	$Na_{12}Phy$ (g/L)	K_2ZrF_6 (g/L)	Treatment Time (min)	P (at.%)	F (at.%)	Zr (at.%)
No. 1	4	8	5	2.5	4.86	33.78	3.13
No. 2	4	12	10	3.0	4.34	22.29	3.49
No. 3	4	16	15	3.5	5.63	12.18	5.38
No. 4	6	8	10	3.5	3.68	28.75	4.04
No. 5	6	12	15	2.5	4.09	29.71	4.48
No. 6	6	16	5	3.0	6.57	26.86	1.84
No. 7	8	8	15	3.0	3.34	34.77	4.58
No. 8	8	12	5	3.5	5.51	28.92	2.15
No. 9	8	16	10	2.5	5.50	29.03	2.53
K_1	14.83 (68.25, 12.00)	11.88 (97.30, 11.75)	16.94 (89.56, 7.12)	14.45 (92.52, 10.14)			
K_2	14.34 (85.32, 10.36)	13.94 (80.92, 10.12)	13.52 (80.07, 10.06)	14.25 (83.92, 9.91)			
K_3	14.35 (92.72, 9.26)	17.70 (68.07, 9.75)	13.06 (76.66, 14.44)	14.82 (69.85, 11.57)			
Difference	0.49 (24.47, 2.74)	5.82 (29.23, 2.00)	3.88 (12.90, 7.32)	0.57 (22.67, 1.66)			
Rank	4 (2, 2)	1 (1, 3)	2 (4, 1)	3 (3, 4)			

2.2. Microstructural Characterization

Surface and cross-sectional morphologies of MAO coatings were observed using a ΣIGMA SEM (Zeiss Sigma, Oberkochen, Germany). The coating compositions were analyzed using an energy dispersive spectrometry (EDS, Oxford INCA, Oberkochen, Germany) attached to an SEM. The phase structure of the oxide film was detected using an X-ray diffractometer (Shimadzu XRD-6100, Tokyo, Japan) with Cu Kα radiation in the 2θ range of 10°–80° at a scanning speed of 4°/min. In order to detect the element states on the surface of the anodic coatings, an X-ray photoelectron spectroscopy (XPS, ESCALAB250, Thermo VG, Waltham, MA, USA) was used with an Al Kα anode (λ = 1486.6 eV).

2.3. Electrochemical Test

Potentiodynamic polarization was measured to measure corrosion current density (I_{corr}) of magnesium alloy before and after MAO treatment using an electrochemical analyzer (CHI660E, Shanghai Chenhua Instrument Co., Ltd., Shanghai, China). All measurements were performed at 37 °C in solutions composed of NH_4HF_2, $Na_{12}Phy$, and/or K_2ZrF_6 as well as a simulated body fluid (SBF) composed of 8 g/L NaCl, 0.4 g/L KCl, 0.14 g/L $CaCl_2$, 0.35 g/L $NaHCO_3$, 1.0 g/L $C_6H_{12}O_6$, 0.2 g/L $MgSO_4 \cdot 7H_2O$, 0.1 g/L KH_2PO_4, and 0.06 g/L $Na_2HPO_4 \cdot 7H_2O$. A three-electrode cell with a sample area of 1 cm^2 was used as the working electrode, a saturated calomel electrode (SCE) as the reference electrode, and a platinum electrode as the counter electrode. The SCE was put into a beaker composed of saturated potassium nitrate while the working and the platinum electrodes were placed into a cell containing SBF. The beaker was connected with the cell by a salt bridge. After an initial delay of 300 s, the potentiodynamic polarization curves were measured from −0.3 to 0.8 V with respect to the open circuit potential (OCP) at a scan rate of 1 mV/s. The corresponding electrochemical parameters including corrosion potential (E_{corr}), I_{corr}, and anodic/cathodic Tafel slopes were derived by using the Tafel extrapolation method. The experiment of each sample was repeated at least three times.

3. Results

3.1. Characteristics of MAO Coatings

3.1.1. Surface Morphology and Chemical Composition

Surface morphologies of the nine MAO coatings were observed and are shown in Figure 1. The MAO coating developed on sample No. 1 was rough and loose with small pore size (Figure 1a), while all other coating samples exhibited uniform and compact porous structure (Figure 1b–i). In addition, micro-cracks shown by arrows were developed on some MAO treated samples, especially on Nos. 6 and 7 (Figure 1f,g). Anodic coatings developed on No. 8 exhibited uniform and compact characteristics with a pore size in the range of 1–4 μm (Figure 1h).

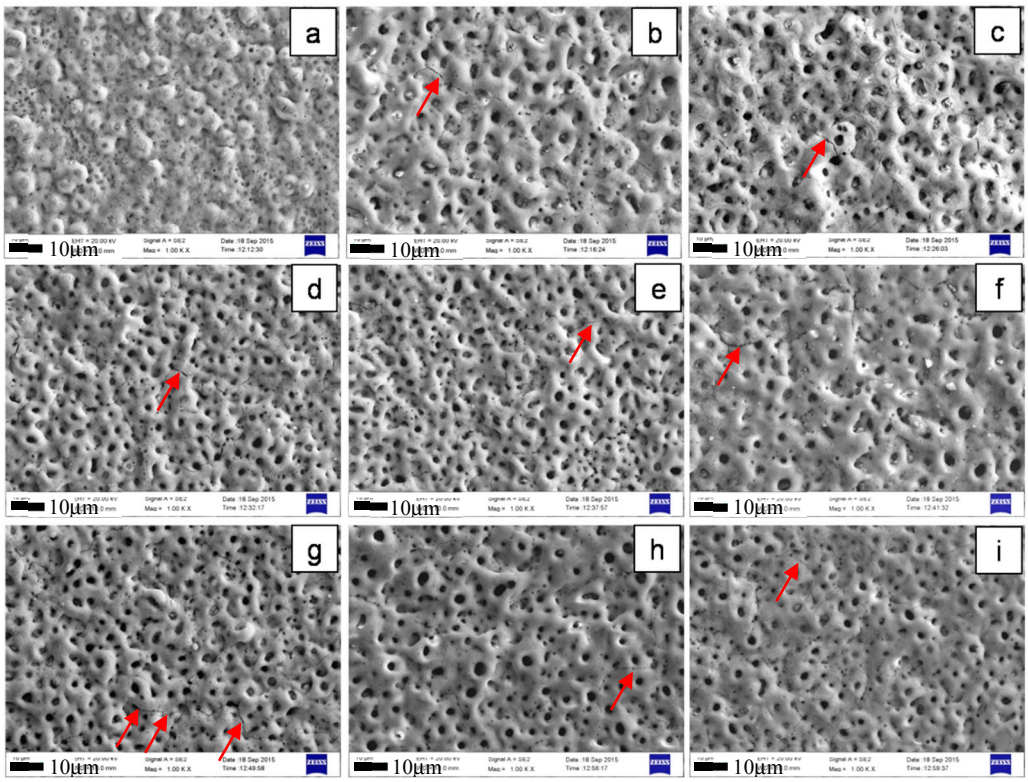

Figure 1. Surface morphologies of anodic films developed on nine micro-arc oxidation (MAO) treated samples: (**a**) No. 1; (**b**) No. 2; (**c**) No. 3; (**d**) No. 4; (**e**) No. 5; (**f**) No. 6; (**g**) No. 7; (**h**) No. 8; and (**i**) No. 9.

Chemical compositions of MAO coatings fabricated in nine processes are listed in Table 2. The MAO coatings were mainly composed of C, O, F, Mg, P, and Zr elements (Table 2). $Na_{12}Phy$ took part in coating formation and phosphorus-containing coatings were developed on the sample surface. The P, F, and Zr contents of each sample are listed in Table 1.

Table 2. Elemental compositions of anodic coatings developed on nine MAO treated samples (at.%).

Process	C	O	F	Mg	P	Zr
No. 1	8.93	28.57	33.78	19.91	4.86	3.13
No. 2	21.54	32.13	22.29	15.27	4.34	3.49
No. 3	14.98	43.93	12.18	16.64	5.63	5.38
No. 4	15.49	28.96	28.75	18.38	3.68	4.04
No. 5	11.89	30.55	29.71	18.10	4.09	4.48
No. 6	9.23	33.50	26.86	20.96	6.57	1.84
No. 7	9.22	27.11	34.77	20.24	3.34	4.58
No. 8	8.81	32.14	28.92	21.31	5.51	2.15
No. 9	10.47	31.48	29.03	19.92	5.50	2.53

3.1.2. Cross-Sectional Morphology

Cross-sectional morphologies of the nine MAO samples are shown in Figure 2. Sample No. 1 exhibited a comparatively uniform and compact microstructure (Figure 2a), while other samples achieved typically porous characteristics with many micro pores (Figure 2b–i). The achieved coating thickness of each sample (Figure 3) is listed in Table 3. Among the nine MAO samples, samples Nos. 3 and 8 achieved the thickest and the second thickest coating, 23.5 and 20.3 μm, respectively. The coating developed on sample No. 1 was the thinnest, only 8.5 μm (Table 3).

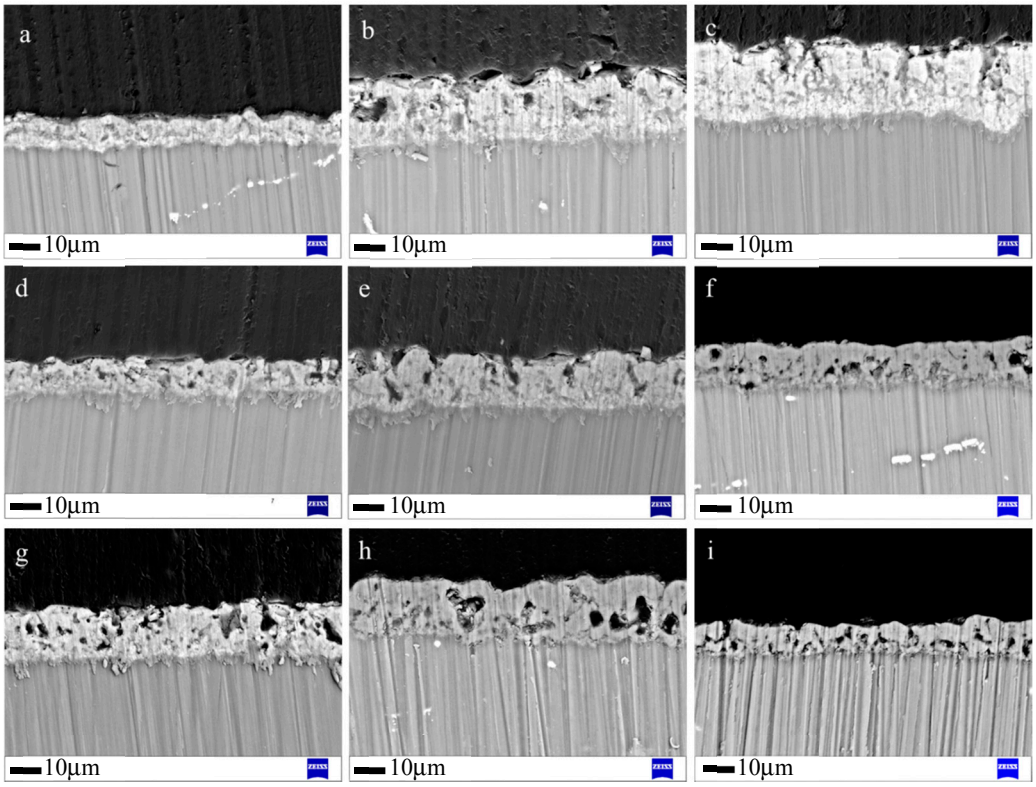

Figure 2. Cross-sectional morphologies of anodic coatings developed on nine MAO treated samples: (**a**) No. 1; (**b**) No. 2; (**c**) No. 3; (**d**) No. 4; (**e**) No. 5; (**f**) No. 6; (**g**) No. 7; (**h**) No. 8; and (**i**) No. 9.

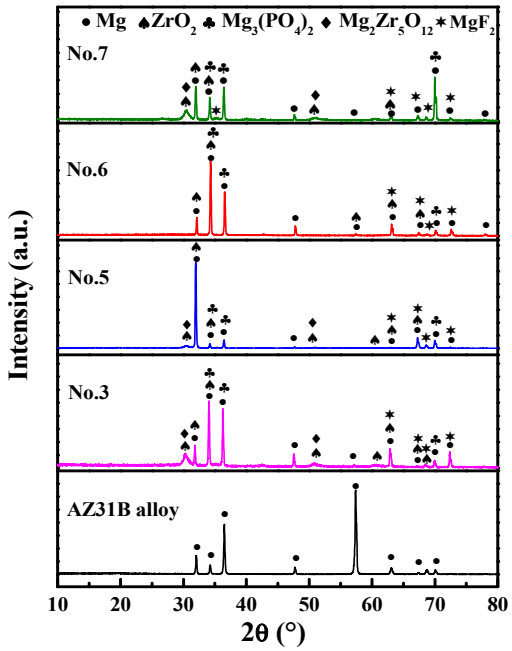

Figure 3. XRD patterns of untreated AZ31B alloy and anodic coatings developed on samples of Nos. 3, 5, 6, and 7.

Table 3. The orthogonal array and experimental results about I_{corr} values and the thickness of MAO treated samples.

Process	NH_4HF_2 (g/L)	$Na_{12}Phy$ (g/L)	K_2ZrF_6 (g/L)	Treatment Time (min)	I_{corr} ($\times 10^{-9}$ A/cm^2)	Thickness (μm)
No. 1	4	8	5	2.5	2.0548	8.5
No. 2	4	12	10	3.0	1.828	19.3
No. 3	4	16	15	3.5	1.4787	23.5
No. 4	6	8	10	3.5	3.2194	10.5
No. 5	6	12	15	2.5	3.6419	17.1
No. 6	6	16	5	3.0	2.2679	18.3
No. 7	8	8	15	3.0	7.8083	16.0
No. 8	8	12	5	3.5	1.8439	20.3
No. 9	8	16	10	2.5	1.7938	9.5
K_1	5.3615 (51.3)	13.0825 (35.0)	6.1666 (47.1)	7.4905 (35.1)		
K_2	9.1292 (45.9)	7.3138 (56.7)	6.8412 (39.3)	11.9042 (53.6)		
K_3	11.446 (45.8)	5.5404 (51.3)	12.9289 (56.6)	6.542 (54.3)		
Difference	6.0845 (5.5)	7.5421 (21.7)	6.7623 (17.3)	5.3622 (19.2)		
Rank	3 (4)	1 (1)	2 (3)	4 (2)		

3.1.3. XRD Analysis

As listed in Table 1, Nos. 3, 5, and 7 contained high Zr contents (5.38, 4.48, and 4.58 at.%), while No. 6 achieved low Zr amount (1.84 at.%). The XRD spectra of untreated AZ31B alloy and the four MAO samples above are displayed in Figure 3. The untreated AZ31B alloy presented typical characteristic peaks of magnesium, while the MAO coatings were mainly composed of Mg, $Mg_3(PO_4)_2$, ZrO_2, $Mg_2Zr_5O_{12}$, and MgF_2.

3.1.4. XPS Analysis

Figure 4 displayed the survey spectrum and high-resolution XPS spectra of C, P, and Zr elements on sample No. 3. The developed MAO coatings on sample No. 3 consisted of C, Mg, O, P, Zr, F, and Al elements (Figure 4a). The C 1*s* spectrum could be divided into two component peaks at 284.6 and 286.5 eV, which were separately assigned to C–C(H) and C–O. The P 2*p* spectrum exhibited two peaks at 133.4 and 134.3 eV (Figure 4c), which represented PO_4^{3-} and HPO_4^{2-}, respectively [37]. The Zr 3*d* spectrum was divided into two peaks at 182.1 and 184.3 eV, corresponding to zirconium oxide [38].

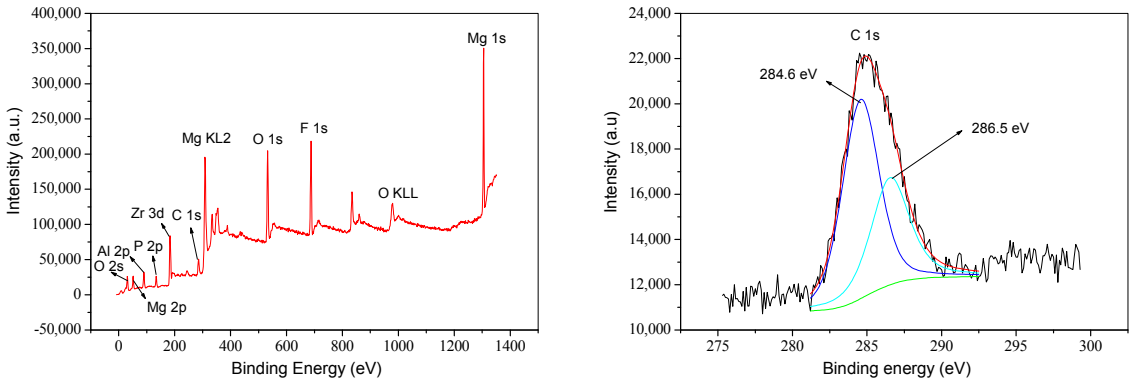

(**a**) (**b**)

Figure 4. *Cont.*

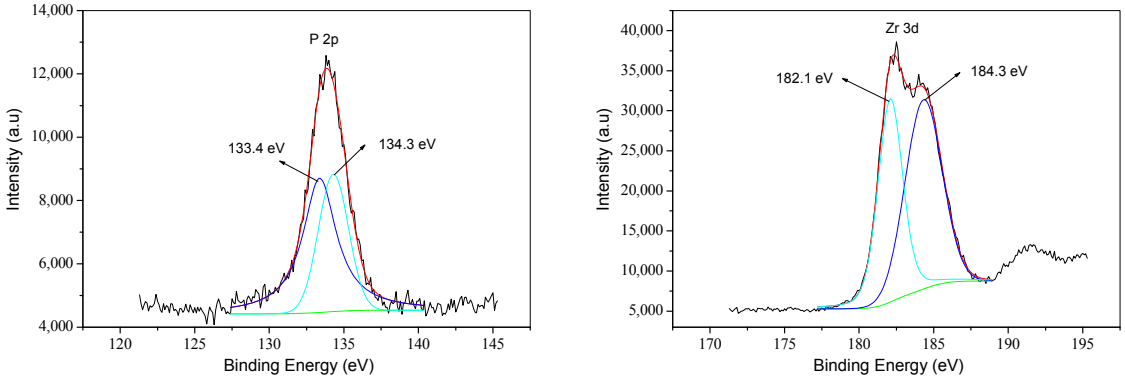

(**c**) (**d**)

Figure 4. X-ray photoelectron spectroscopy (XPS) spectra of anodic coatings developed on sample No. 3: (**a**) survey; (**b**) C 1*s*; (**c**) P 2*p*; (**d**) Zr 3*d*.

3.1.5. Corrosion Resistance

Figure 5 shows the potentiodynamic polarization curves of untreated AZ31B alloy and the nine MAO treated samples. Derived from Figure 6, the electrochemical parameters of the tested sample could be achieved. The E_{corr} and the I_{corr} of AZ31B alloy were −1.5287 V (vs. SCE) and 4.06×10^{-6} A/cm^2, respectively. The achieved I_{corr} values of the nine MAO treated samples are listed in Table 3. The I_{corr} value reflects the corrosion resistance of the measured sample. The smaller the I_{corr} value, the better the corrosion resistance. Compared with untreated AZ31B alloy, it was clear that all MAO samples achieved smaller I_{corr} values (Table 3), indicating that the MAO treatment could effectively improve the corrosion resistance of the AZ31B alloy. Among the nine samples, sample No. 3 exhibited the best corrosion resistance, and its I_{corr} (1.48×10^{-9} A/cm^2) was three orders of magnitude smaller than that of untreated AZ31B alloy.

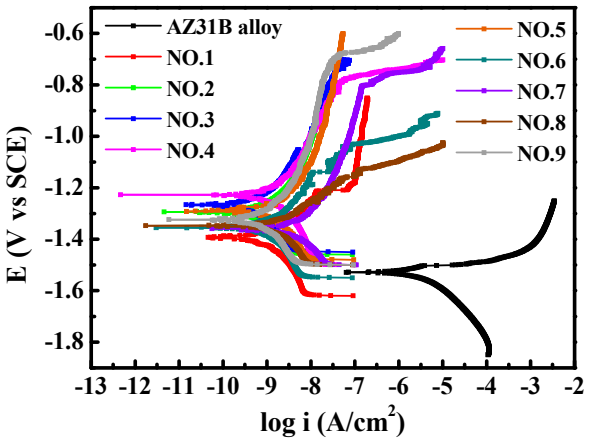

Figure 5. Potentiodynamic polarization curves of untreated AZ31B alloy and nine MAO treated samples measured in simulated body fluid (SBF).

3.2. The Orthogonal Results

3.2.1. Influences of Processing Factors on P, F and Zr Contents

The measured P, F, and Zr contents of the MAO coatings were set as the objective parameters, and the intuitionistic analysis was used to analyze the experimental data and reveal the influences of processing factors on the objective parameters. K_1, K_2, and K_3 in Table 1 separately represent objective parameter summation of MAO coatings fabricated at the first, second, and third levels for each of the four processing factors. The maximum difference between K_1, K_2, and K_3 for each factor reflects the

general effect of that factor. Based on this point of view, the influencing ranks of four processing factors on P, F, and Zr content were separately: $Na_{12}Phy$ concentration > K_2ZrF_6 concentration > treatment time > NH_4HF_2 concentration; $Na_{12}Phy$ concentration > NH_4HF_2 concentration > treatment time > K_2ZrF_6 concentration; and K_2ZrF_6 concentration > NH_4HF_2 concentration > $Na_{12}Phy$ concentration > treatment time (Table 1). Obviously, $Na_{12}Phy$ was the primary contributing factor to the P and F contents, and K_2ZrF_6 mainly determined the Zr content of MAO coatings.

The influence of the four processing factors on the P, F, and Zr contents are shown in Figure 6. In detail, with the increasing NH_4HF_2 concentration, the P and Zr amounts decreased while the F amount continually increased. The increasing $Na_{12}Phy$ concentration considerably increased the P but decreased both F and Zr amounts. With the increase of K_2ZrF_6 concentration, the Zr contents increased progressively, while the P and F contents decreased gradually. Moreover, with the extension of treatment time, the F amount in anodic coatings continually decreased, while the P and Zr contents firstly decreased from Level 1 to Level 2 but then slightly increased from Level 2 to Level 3. These results showed that P, F, and Zr competed with each other to enter into MAO coatings.

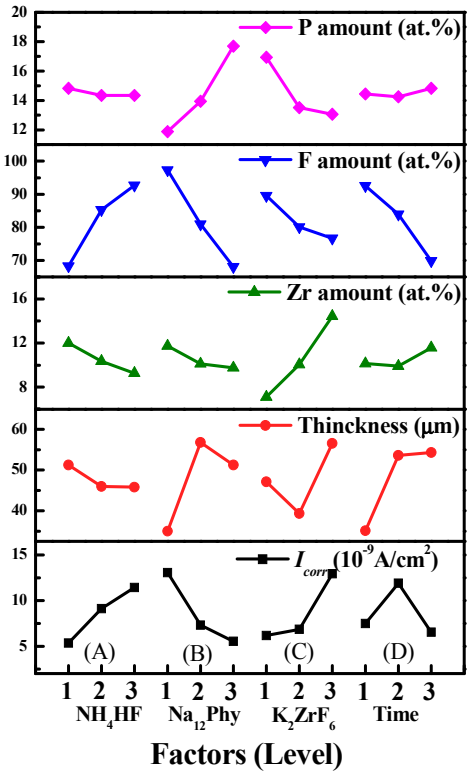

Figure 6. The influences of the processing parameters on the P, F, Zr contents, and the coating thickness and I_{corr}: (**A**) NH_4HF_2 concentration; (**B**) $Na_{12}Phy$ concentration; (**C**) K_2ZrF_6 concentration; and (**D**) treatment time.

3.2.2. Influences of Processing Factors on Corrosion Resistance and Thickness

The I_{corr} values of nine MAO samples derived from the potentiodynamic polarization curves in Figure 5 are listed in Table 3 and were selected as the objective parameter for corrosion evaluation. According to the intuitionistic analysis results shown in Table 2, the rank of processing factors on I_{corr} of the MAO samples was $Na_{12}Phy$ concentration > K_2ZrF_6 concentration > NH_4HF_2 concentration > treatment time. Based on Table 3, the influences of the four factors on I_{corr} value are shown in Figure 6.

The change trends of I_{corr} values with the four processing factors are shown in Figure 6. With the increasing NH_4HF_2 concentration, the I_{corr} values significantly increased, and therefore the corrosion resistance of MAO coatings evidently decreased. However, with the increase of $Na_{12}Phy$ concentration, the I_{corr} values decreased gradually, suggesting that $Na_{12}Phy$ was definitely beneficial to enhancing

the corrosion resistance of the MAO coating. With the increase of K_2ZrF_6 concentration, the I_{corr} values of the MAO samples slightly increased from Level 1 to Level 2 but then significantly increased from Level 2 to Level 3 (Figure 6), indicating that excess high K_2ZrF_6 was harmful to the coating corrosion resistance. Treatment time was the least important factor on I_{corr} value, and the I_{corr} firstly increased from Level 1 to Level 2 but then decreased from Level 2 to Level 3 (Figure 6).

The influencing sequence of four processing factors on the coating thickness was $Na_{12}Phy$ concentration > treatment time > K_2ZrF_6 concentration > NH_4HF_2 concentration (Table 3). The change trends of the coating thickness with four factors are shown in Figure 6. With the increasing $Na_{12}Phy$ concentration, the MAO coating first increased and then slowly decreased. With the prolongation of treatment time, the coating thickness gradually increased. K_2ZrF_6 firstly decreased but then increased the coating thickness, while the increasing NH_4HF_2 concentration presented a slightly decreased coating thickness.

The correlation between the I_{corr} values and coating characteristics such as thickness, P, F, and Zr amounts is shown in Figure 7. It was clear that except Nos. 4 and 5, the coating thickness exhibited a negative effect on I_{corr} values of the MAO treated alloy. On the contrary, the F amount in the MAO coatings exhibited a positive effect on I_{corr} values. However, the interrelation between I_{corr} and the amounts of P and Zr in MAO coatings remained unclear (Figure 7).

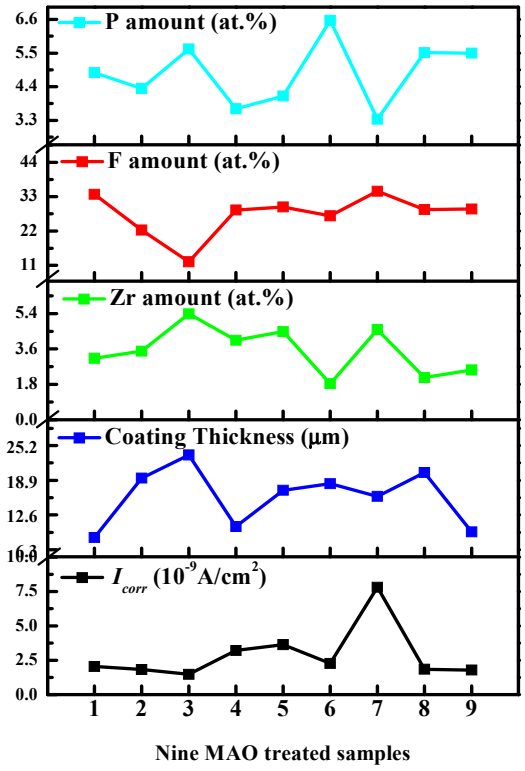

Figure 7. The correlation between I_{corr} of nine MAO treated samples with P, F, and Zr amounts and coating thickness.

3.3. Influences of Electrolyte Components on Coating Development

As shown in Figure 1a, MAO coating developed on No. 1 was fabricated in the solution composed of 4 g/L NH_4HF_2, 8 g/L $Na_{12}Phy$, and 5 g/L K_2ZrF_6 with a treatment time of 2.5 min. In order to clarify the influences of NH_4HF_2, $Na_{12}Phy$, and K_2ZrF_6 on coating development, surface morphologies of the MAO treated samples fabricated in solutions composed of one, two, or three electrolyte solutions and the I_{corr} values of untreated AZ31B alloy measured in corresponding solutions are shown in Figure 8.

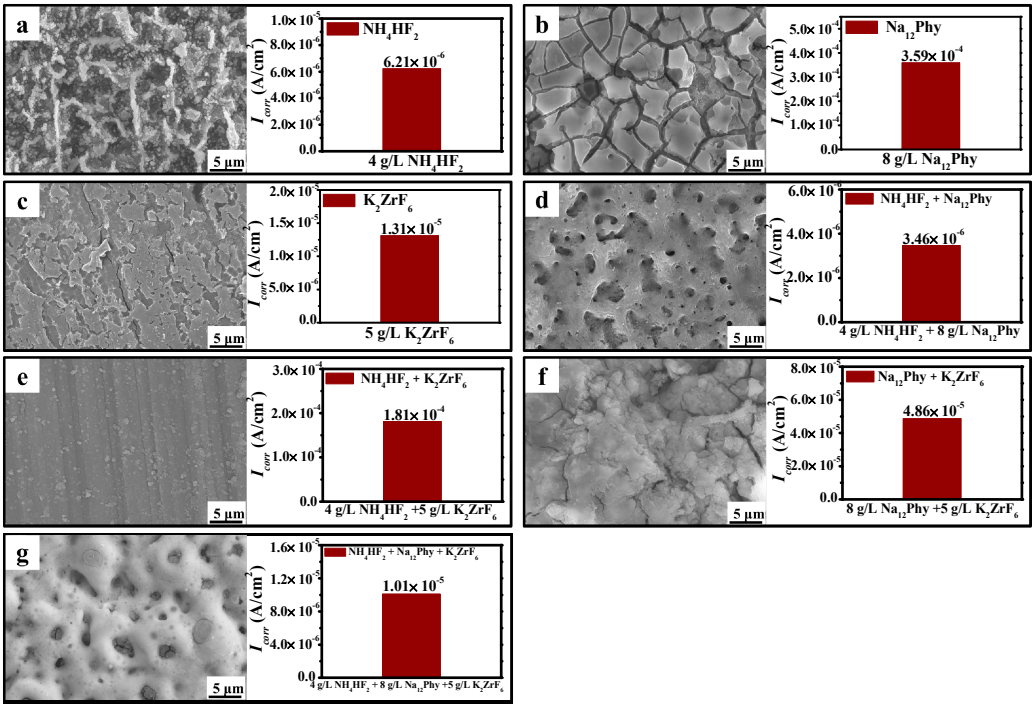

Figure 8. Surface morphologies of anodic films fabricated in different solutions and the I_{corr} values of AZ31B alloy in corresponding solutions: (**a**) 4 g/L NH_4HF_2; (**b**) 8 g/L $Na_{12}Phy$; (**c**) 5 g/L K_2ZrF_6; (**d**) 4 g/L NH_4HF_2 + 8 g/L $Na_{12}Phy$; (**e**) 4 g/L NH_4HF_2 + 5 g/L K_2ZrF_6; (**f**) 8 g/L $Na_{12}Phy$ + 5 g/L K_2ZrF_6; and (**g**) 4 g/L NH_4HF_2 + 8 g/L $Na_{12}Phy$ + 5 g/L K_2ZrF_6.

In a solution of 4 g/L NH_4HF_2, anodic coatings with rough characteristics were developed on a magnesium surface (Figure 8a). I_{corr} measured in the solution was 6.21 × 10^{-6} A/cm^2. During MAO treatment in 8 g/L $Na_{12}Phy$, the working voltage increased very slowly and reached 161 V after 2.5 min. Observed by SEM, the fabricated film achieved evident cracks (Figure 8b). The tested I_{corr} in 8 g/L $Na_{12}Phy$ was 2.31 × 10^{-5} A/cm^2, evidently larger than that in 4 g/L NH_4HF_2. However, in the solution of 5 g/L K_2ZrF_6, the working voltage firstly increased slowly to 96 V but then fluctuated at about 60 V. Anodic coatings could not develop, and I_{corr} in the solution was 1.58 × 10^{-5} A/cm^2 (Figure 8c).

In solutions composed of two electrolyte components, the AZ31B samples were MAO treated, and the results are shown in Figure 8d–f. In the solution composed of 4 g/L NH_4HF_2 + 8 g/L $Na_{12}Phy$, the working voltage reached 295 V after 2.5 min, and the fabricated coatings exhibited typically porous structure (Figure 8d). However, it was evident that in solutions composed of 4 g/L NH_4HF_2 + 5 g/L K_2ZrF_6 and 8 g/L $Na_{12}Phy$ + 5 g/L K_2ZrF_6, anodic coatings could not develop on magnesium alloy (Figure 8e,f). After 5 g/L K_2ZrF_6 was added into the solution of 4 g/L NH_4HF_2 + 8 g/L $Na_{12}Phy$, the developed MAO coatings achieved self-sealing characteristics (Figure 1a or Figure 8g), demonstrating that K_2ZrF_6 played a sealing role on anodic coatings. I_{corr} values measured in solutions of 4 g/L NH_4HF_2 + 8 g/L $Na_{12}Phy$, 4 g/L NH_4HF_2 + 5 g/L K_2ZrF_6, and 8 g/L $Na_{12}Phy$ + 5 g/L K_2ZrF_6 were separately 3.46 × 10^{-6}, 1.81 × 10^{-4}, and 4.86 × 10^{-5} A/cm^2, while I_{corr} obtained in 4 g/L NH_4HF_2 + 8 g/L $Na_{12}Phy$ + 5 g/L K_2ZrF_6 was 1.01 × 10^{-5} A/cm^2 (Figure 8g). The results showed that coating development on magnesium alloy in a used solution was determined by electrolyte component and I_{corr} of untreated AZ31B measured in the solution. In general, anodic coatings fabricated in the solution with a low I_{corr} achieved good property.

4. Discussion

4.1. The Entrance Mechanisms of P, F, and Zr into MAO Coatings

Formation of MAO coatings on valve metals is a complex process potentially involving anodic oxidation, thermal oxidation, and plasma-chemical reactions [19]. In this study, the development of anodic coatings containing P, F, and Zr can be classified into two stages, as shown in Figure 9. In the first stage, the ionization of the used electrolytes occurs. For example, $Na_{12}Phy$ is ionized into phytic acid radicals (IP6), while NH_4HF_2 can be ionized into NH_4^+, HF, and F^- (shown as red circle in Figure 9):

$$NH_4HF_2 = NH_4^+ + HF + F^- \quad (1)$$

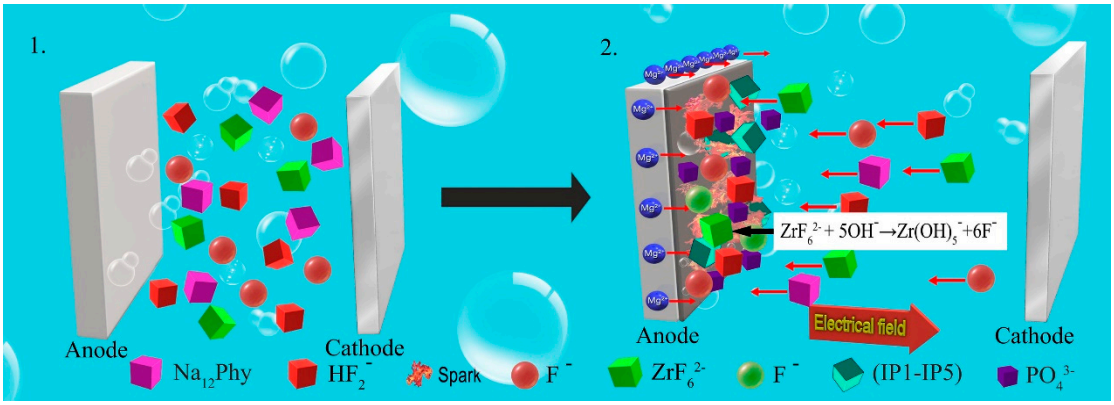

Figure 9. The schematic diagram of P, F, and Zr into MAO coatings. Illustrations: the red F^- comes from NH_4HF_2; the green F^- comes from K_2ZrF_6; (IP1–IP5) is the lower inositol phosphate ester due to the hydrolysis of $Na_{12}Phy$.

In the second stage, namely MAO, work voltage continually increases, and moving sparks appear on the sample surface. In this stage, a magnesium alloy sample is oxidized into Mg^{2+}:

$$Mg - 2e^- = Mg^{2+} \quad (2)$$

During MAO, an electric field develops between the anode and the cathode, driving anions such as F^-, OH^-, phytic acid radicals, and ZrF_6^{2-} towards the anode [12,39]. When these anions arrive at the anode, they compete against each other to combine with Mg^{2+} and develop stable ceramic coatings under instantaneous high temperature and high pressure. As listed in Table 2, the fabricated anodic coating contains P, which originates from $Na_{12}Phy$. $Na_{12}Phy$ is an organic phosphorus-containing substance and remains stable at low temperatures. However, $Na_{12}Phy$ can be hydrolyzed between temperatures of 320 and 345 °C [40]. During MAO, the instantaneous high temperature on the anode surface due to sparks discharging can result in the hydrolysis of $Na_{12}Phy$ into phosphorylated myo-myo-inositols (IP1–IP5) and inorganic phosphate [41], which may include the following equations:

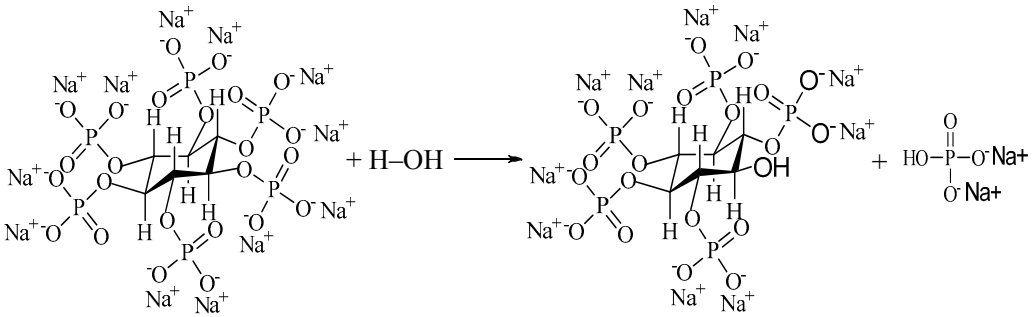

(3)

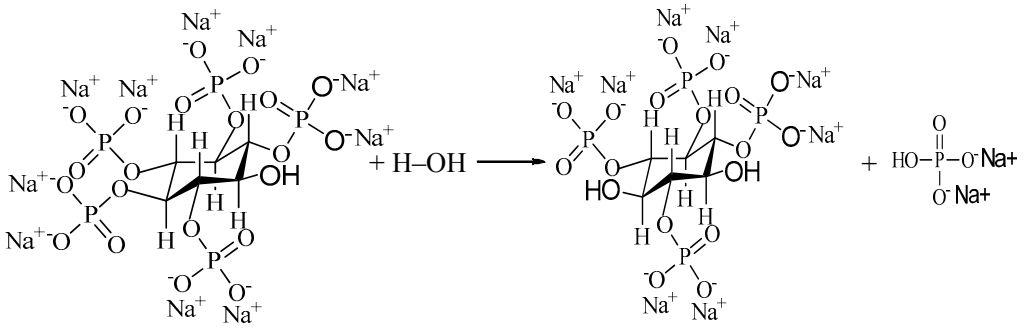

(4)

PO_4^{3-} ions (produced from the hydrolysis of $Na_{12}Phy$) combine with Mg^{2+} (from the oxidation of magnesium) to be converted into stable $Mg_3(PO_4)_2$:

$$3Mg^{2+} + 2PO_4^{3-} = Mg_3(PO_4)_2 \quad (5)$$

Besides P element, F and Zr are also incorporated into the MAO coatings. F in MAO coatings comes from both NH_4HF_2 and K_2ZrF_6, while Zr originates from K_2ZrF_6. K_2ZrF_6, a complex electrolyte containing both F and Zr elements, is the most important factor on Zr content but is the least important factor on F content (Table 1). In a solution containing NH_4HF_2 and K_2ZrF_6, the following reactions may be involved [18,19]:

$$5OH^- + ZrF_6^{2-} = Zr(OH)_5^- + 6F^- \quad (6)$$

$$5Zr(OH)_5^- + 2Mg^{2+} = Mg_2Zr_5O_{12} + 12H_2O + OH^- \quad (7)$$

$$Zr(OH)_5^- = ZrO_2 + 2H_2O + OH^- \quad (8)$$

$$2F^- + Mg^{2+} = MgF_2 \quad (9)$$

During MAO, $Zr(OH)_5^-$ and F^- (shown as green circle in Figure 9) are firstly obtained from ZrF_6^{2-} according to Equation (6). Then, $Zr(OH)_5^-$ ions take part in the coating formation by converting into $Mg_2Zr_5O_{12}$ or ZrO_2 in MAO coatings (Equations (7) and (8)). F^- ions are mainly combined with Mg^{2+} to develop stable MgF_2 (Equation (9)). Therefore, Zr and F from K_2ZrF_6 compete with each other to take part in the coating formation.

The solubility of the developed products is a main factor in determining the combination sequence of these anions with Mg^{2+} ion. At 298.15 K, the solubility product constant (K_{sp}) of magnesium phosphate and magnesium fluoride are 10^{-27}–10^{-23} and 6.5×10^{-9}, respectively [42]. PO_4^{3-} ions preferentially combine with Mg^{2+} to develop stable $Mg_3(PO_4)_2$ (Equation (5)). Therefore, $Na_{12}Phy$ is the important factor contributing to the F and Zr contents, and the increasing $Na_{12}Phy$ concentration decreases both F and Zr amounts in MAO coatings.

Compared with K_2ZrF_6, NH_4HF_2 plays a larger role on the F amount (Table 1). The reason behind this may result from the different moving speed of HF_2^- or F^- from NH_4HF_2 and ZrF_6^{2-} from K_2ZrF_6 in a water solution. Due to a comparatively large spatial structure [43], ZrF_6^{2-} moves slower in a water solution than HF_2^- or F^-. As shown in Figure 7, with the increasing K_2ZrF_6 concentration, the Zr amount in anodic coatings increases significantly, while the F amount slowly decreases. The reasoning may be that the reaction of ZrF_6^{2-} combining with OH^- into $Zr(OH)_5^-$ and F^- takes place near the anode (Figure 9). The electric field causes the ZrF_6^{2-} ions to move slowly toward the anode. After arriving at the anode, ZrF_6^{2-} ions combine with OH^- into $Zr(OH)_5^-$ and F^- under high temperatures due to sparks discharging (Equation (6)). Next, $Zr(OH)_5^-$ and F^- separately enter into anodic coatings, according to Equations (7)–(9). Because of the slower ZrF_6^{2-} speed compared to that of HF_2^- or F^- (Figure 9) and the late reaction of ZrF_6^{2-} into $Zr(OH)_5^-$ and F^-, the F^- from ZrF_6^{2-} has less influence on the F amount than F^- from NH_4HF_2. In contrast, the obtained $Zr(OH)_5^-$ from ZrF_6^{2-} can develop into considerable amounts of $Mg_2Zr_5O_{12}$ and ZrO_2 (Equations (7) and (8)), resulting in the comparative decrease of F element in anodic coatings.

The used electrolytes should first arrive at the anode by diffusion or electromigration and then enter into MAO coatings through a serious of chemical reactions. Cations move to the anode mainly by diffusion, while anions can arrive at the anode by both diffusion and electromigration. Between the moving speed and reaction speed, the slower step determines the amount that develops in MAO coatings. Treatment time can affect the coating compositions by determining the intensity of the electric field. With a prolonged treatment time, the electric field becomes stronger, and therefore the anions in the solution move faster toward the anode [12,39]. In this study, P, F, and Zr compete with each other to enter anodic coatings, causing a complex influencing mechanism of treatment time on coating compositions. F^- ions move quickly due to their comparatively small spatial structure [44], resulting in the F amount in anodic coatings to be mainly determined by reaction speed. In contrast, the P and Zr amounts are mainly determined by the movement speed of phytic acid radicals and ZrF_6^{2-}. Therefore, the prolonged treatment time is helpful for improving the P and Zr amounts but decreases the F amount. When treatment time is prolonged from 3.0 to 3.5 min, the Zr amount slightly decreases (Table 1). The reason may be that under this condition, the Zr amount increases slower than the P amount, and therefore the Zr amount comparatively decreases.

4.2. Influence of Processing Factors on Corrosion Resistance

The corrosion resistance of the fabricated MAO samples is jointly determined by coating characteristics such as coating thickness, surface morphology, phase structure, and the used substrate [3,9,11,13,14,16,17,19,36,44–46]. The thick MAO coating with a uniform surface, a compact inner layer, and chemically stable components can effectively prevent the corrosion solution from penetrating the coating and reacting with magnesium substrate. Among coating characteristics, coating thickness plays an important role in its corrosion resistance. With increasing coating thickness, the corrosion resistance of MAO treated samples increases [13,14]. Besides coating thickness, surface morphology such as micro-cracks, micro pore size, and porosity can effectively influence the corrosion resistance of MAO treated magnesium alloys [3,13,17,45,46]. For example, with an increasing KOH concentration, through porosity also increases and corrosion resistance decreases [46].

In this study, the changing regularity of P and Zr amounts with that of I_{corr} is not clear (Figure 7), indicating that the influences of P and Zr on the corrosion resistance is not fixed. According to Figure 8, the coating thickness and the F amount in MAO coatings are approximately closely related with I_{corr} of MAO treated samples. With the increased coating thickness, the MAO coatings achieve decreased I_{corr} and therefore good corrosion resistance. However, sample No. 7 achieves the worst corrosion resistance, yet its coating thickness is not the thinnest (Table 3), indicating that besides coating thickness, other factors such as chemical compositions and surface morphology of MAO coatings can also influence the corrosion resistance.

NH_4HF_2, an acidic fluorine-containing substance, is usually used as a corrosion inhibitor for magnesium alloy in electroless nickel plating [33,34]. The measured I_{corr} in 4 g/L NH_4HF_2 is very low and anodic coatings can be developed in the solution (Figure 8a). As listed in Tables 1 and 2, the increasing NH_4HF_2 concentration significantly increases the F amount but decreases the coating thickness and corrosion resistance (Table 3). These results indicate that NH_4HF_2 is beneficial for the coating formation and takes part in coating formation. However, compared with $Na_{12}Phy$, K_2ZrF_6, or treatment time, NH_4HF_2 has little influence on coating thickness and therefore continually decreases the corrosion resistance.

$Na_{12}Phy$ or phytic acid is a corrosion inhibitor of copper [47], aluminum alloy [48], and magnesium alloy [34]. The results show that $Na_{12}Phy$ promotes the formation of a passive film but is not a suitable candidate for the inhibition of copper corrosion due to its low inhibition efficiency [47]. Compared with NH_4HF_2 or K_2ZrF_6, I_{corr} measured in 8 g/L $Na_{12}Phy$ is the largest, but anodic coatings with many cracks are developed on AZ31B alloy (Figure 8b). After 4 g/L NH_4HF_2 is added into the solution of 8 g/L $Na_{12}Phy$, the measured I_{corr} is very small and uniform, and compact MAO coatings

are developed on magnesium alloys (Figure 8d). As listed in Table 3, $Na_{12}Phy$ can significantly increase the coating thickness and therefore improve the corrosion resistance.

Unlike NH_4HF_2 or $Na_{12}Phy$, K_2ZrF_6 is not an inhibitor of magnesium alloys [33]. In a solution containing 5 g/L K_2ZrF_6, the coating cannot develop (Figure 8c), which may be due to the acidic characteristics of K_2ZrF_6. After 4 g/L NH_4HF_2 or 8 g/L $Na_{12}Phy$ is added into the solution of 5 g/L K_2ZrF_6, anodic coatings still cannot develop (Figure 8e,f), demonstrating that K_2ZrF_6 belongs to the corrosive agent of magnesium alloys. In fact, ZrF_6^{2-} is usually used to develop a conversion film on magnesium alloys [49]. Only under the combined action of NH_4HF_2 and $Na_{12}Phy$ can K_2ZrF_6 take part in coating formation and develop self-sealing coatings. K_2ZrF_6 plays a positive and a negative role on coating corrosion resistance. On the one hand, the fabricated MAO samples in solutions containing K_2ZrF_6 achieve excellent corrosion resistance due to the superior stability of ZrO_2 [16] and the developed self-sealing coatings [17–19]. On the other hand, surface cracks develop on MAO coating in solutions containing K_2ZrF_6 [17,18]. As listed in Table 2, when $Na_{12}Phy$, NH_4HF_2, $Na_{12}Phy$, and treatment time are separately at Level 1, Level 3, Level 3, and Level 2, the fabricated sample No. 7 achieves the worst corrosion resistance, which may be attributed to the evident micro-cracks (Figure 1g) and rough microstructure (Figure 2g). Therefore, with the increase of K_2ZrF_6 concentration, the corrosion resistance slightly decreases from 5 to 10 g/L but significantly deteriorates from 10 to 15 g/L (Table 3).

5. Conclusions

P and F are essential elements of human beings, while zirconium oxides are bioinert with good biocompatibility. The influences of NH_4HF_2, $Na_{12}Phy$, and K_2ZrF_6 concentrations as well as treatment time on the corrosion resistance of MAO treated samples were systematically investigated using the orthogonal method. In addition, the entrance mechanisms of P, F, and Zr into MAO coatings were discussed. The developed anodic coatings can effectively improve the corrosion resistance of magnesium alloys. Some conclusions are as follows:

- NH_4HF_2, $Na_{12}Phy$, and K_2ZrF_6 all partake in the coating formation, and the fabricated MAO coatings are mainly composed of $Mg_3(PO_4)_2$, ZrO_2, $Mg_2Zr_5O_{12}$, and MgF_2. NH_4HF_2 and $Na_{12}Phy$, the corrosion inhibitors of magnesium alloys, are beneficial but K_2ZrF_6 is harmful to develop anodic coatings. Only under the combined action of NH_4HF_2 and $Na_{12}Phy$ can K_2ZrF_6 take part in coating formation and develop self-sealing coatings;
- The corrosion resistance of MAO coatings is synergistically determined by coating characteristics such as coating thickness, surface morphology, and phase structure, though the coating thickness plays a main role. $Na_{12}Phy$ significantly improves but NH_4HF_2 decreases the corrosion resistance of MAO coatings, while excess high K_2ZrF_6 is harmful to the coating corrosion resistance. Treatment time can increase the coating thickness but is the least important factor on corrosion resistance;
- P, F, and Zr compete with each other to enter into anodic coatings. The influencing rank on P content is $Na_{12}Phy$ concentration > K_2ZrF_6 concentration > treatment time > NH_4HF_2 concentration. With the increase of $Na_{12}Phy$ or the decrease of K_2ZrF_6 concentration, the P amount of anodic coatings increases. The sequence of processing factors on F content is $Na_{12}Phy$ concentration > NH_4HF_2 concentration > treatment time > K_2ZrF_6 concentration. The F amount decreases with the increasing $Na_{12}Phy$ concentration, decreasing NH_4HF_2 concentration, prolonging treatment time, or increasing K_2ZrF_6 concentration. The order on the Zr amount is K_2ZrF_6 concentration > NH_4HF_2 concentration > $Na_{12}Phy$ concentration > treatment time. The Zr content can be increased by increasing K_2ZrF_6 concentration, decreasing NH_4HF_2 and $Na_{12}Phy$ concentrations, or with proper treatment.

Author Contributions: Conceptualization, R.Z. (Rongfa Zhang) and Y.S.; Software, G.L.; Formal Analysis, H.H.; Investigation, W.C. and Y.Z. (Yijia Zhang); Data Curation, S.Z.; Writing—Original Draft Preparation, Y.Z. (Yuanyuan Zhu) and W.C.; Writing—Review and Editing, R.Z. (Rongfang Zhao) and R.Z. (Rongfa Zhang).

Funding: This study was funded by the National Natural Science Foundation of China (Nos. 51361011 and 51861007).

Acknowledgments: We appreciate the valuable comments provided by other members of our laboratories.

Conflicts of Interest: The authors declare no conflict of interest.

References

1. El-Sayed, M.; El-Hadidi, M.; El-Adl, W. Free non-vascularised fibular graft for treatment of post-traumatic bone defects. *Acta Orthop. Belg.* **2007**, *73*, 70–76.
2. Narayanan, T.S.; Park, I.S.; Lee, M.H. Strategies to improve the corrosion resistance of microarc oxidation (MAO) coated magnesium alloys for degradable implants: Prospects and challenges. *Prog. Mater. Sci.* **2014**, *60*, 1–71. [CrossRef]
3. Han, J.J.; Wan, P.; Sun, Y.; Liu, Z.Y.; Fan, X.M.; Tan, L.L.; Yang, K. Fabrication and evaluation of a bioactive Sr–Ca–P contained micro-arc oxidation coating on magnesium strontium alloy for bone repair application. *J. Mater. Sci. Technol.* **2016**, *32*, 233–244. [CrossRef]
4. Krishna, L.R.; Sundararajan, G. Aqueous corrosion behavior of micro-arc oxidation (MAO)-coated magnesium alloys: A critical review. *JOM* **2014**, *66*, 1045–1060. [CrossRef]
5. Cerchier, P.; Pezzato, L.; Brunelli, K.; Dolcet, P.; Bartolozzi, A.; Bertani, R.; Dabalà, M. Antibacterial effect of PEO coating with silver on AA7075. *Mater. Sci. Eng. C* **2017**, *75*, 554–564. [CrossRef]
6. Mohedano, M.; Guzman, R.; Arrabal, R.; López Lacomba, J.L.; Matykina, E. Bioactive plasma electrolytic oxidation coatings-the role of the composition, microstructure, and electrochemical stability. *J. Biomed. Mater. Res. B Appl. Biomater.* **2013**, *101*, 1524–1537. [CrossRef]
7. Xu, J.L.; Xiao, Q.F.; Mei, D.D.; Tong, Y.X.; Zheng, Y.F.; Li, L.; Zhong, Z.C. Microstructure, corrosion resistance and formation mechanism of alumina micro-arc oxidation coatings on sintered NdFeB permanent magnets. *Surf. Coat. Technol.* **2017**, *309*, 621–627. [CrossRef]
8. Wang, Y.M.; Wang, F.H.; Xu, M.J.; Zhao, B.; Guo, L.X.; Ouyang, J.H. Microstructure and corrosion behavior of coated AZ91 alloy by microarc oxidation for biomedical application. *Appl. Surf. Sci.* **2009**, *255*, 9124–9131. [CrossRef]
9. Cui, L.Y.; Zeng, R.C.; Guan, S.K.; Qi, W.C.; Zhang, F.; Li, S.Q.; Han, E.H. Degradation mechanism of micro-arc oxidation coatings on biodegradable Mg–Ca alloys: The influence of porosity. *J. Alloy. Compd.* **2017**, *695*, 2464–2476. [CrossRef]
10. Verdier, S.; Boinet, M.; Maximovitch, S.; Dalard, F. Formation, structure and composition of anodic films on AM60 magnesium alloy obtained by DC plasma anodizing. *Corros. Sci.* **2005**, *47*, 1429–1444. [CrossRef]
11. Chu, C.L.; Han, X.; Bai, J.; Xue, F.; Chu, P.K. Fabrication and degradation behavior of micro-arc oxidized biomedical magnesium alloy wires. *Surf. Coat. Technol.* **2012**, *213*, 307–312. [CrossRef]
12. Guo, S.B.; Zhang, Y.Q.; Zhang, R.F.; Zhang, S.F.; Zhang, H.H. Influence of processing factors on properties of anodic coatings obtained on Mg–1.0Ca alloy. *Mater. Chem. Phys.* **2013**, *141*, 121–127. [CrossRef]
13. Jia, Z.J.; Li, M.; Liu, Q.; Xu, X.C.; Cheng, Y.; Zheng, Y.F.; Xi, T.F.; Wei, S.C. Micro-arc oxidization of a novel Mg-1Ca alloy in three alkaline KF electrolytes: Corrosion resistance and cytotoxicity. *Appl. Surf. Sci.* **2014**, *292*, 1030–1039. [CrossRef]
14. Lin, X.; Yang, X.M.; Tan, L.L.; Li, M.; Wang, X.; Zhang, Y.; Yang, K.; Hua, Z.Q.; Qiu, J.H. In vitro degradation and biocompatibility of a strontium-containing micro-arc oxidation coating on the biodegradable ZK60 magnesium alloy. *Appl. Surf. Sci.* **2014**, *288*, 718–726. [CrossRef]
15. Fischerauer, S.F.; Kraus, T.; Wu, X.; Tangl, S.; Sorantin, E.; Hänzi, A.C.; Löffler, J.F.; Uggowitzer, P.J.; Weinberg, A.M. In vivo degradation performance of micro-arc-oxidized magnesium implants: A micro-CT study in rats. *Acta Biomater.* **2013**, *9*, 5411–5420. [CrossRef] [PubMed]
16. Liang, J.; Srinivasan, P.B.; Blawert, C.; Dietzel, W. Comparison of electrochemical corrosion behaviour of MgO and ZrO_2 coatings on AM60 magnesium alloy formed by plasma electrolytic oxidation. *Corros. Sci.* **2009**, *51*, 2483–2492. [CrossRef]

17. Liu, F.; Shan, D.Y.; Song, Y.W.; Han, E.H. Effect of additives on the properties of plasma electrolytic oxidation coatings formed on AM50 magnesium alloy in electrolytes containing K_2ZrF_6. *Surf. Coat. Technol.* **2011**, *206*, 455–463. [CrossRef]
18. Einkhah, F.; Lee, K.M.; Sani, M.A.F.; Yoo, B.; Shin, D.H. Structure and corrosion behavior of oxide layer with Zr compounds on AZ31 Mg alloy processed by two-step plasma electrolytic oxidation. *Surf. Coat. Technol.* **2014**, *238*, 75–79. [CrossRef]
19. Cui, X.J.; Liu, C.H.; Yang, R.S.; Li, M.T.; Lin, X.Z. Self-sealing micro-arc oxidation coating on AZ91D Mg alloy and its formation mechanism. *Surf. Coat. Technol.* **2015**, *269*, 228–237. [CrossRef]
20. Luo, H.H.; Cai, Q.Z.; Wei, B.K.; Yu, B.; He, J.; Li, D.J. Study on the microstructure and corrosion resistance of ZrO_2-containing ceramic coatings formed on magnesium alloy by plasma electrolytic oxidation. *J. Alloy. Compd.* **2009**, *474*, 551–556. [CrossRef]
21. Wang, S.M.; Fu, L.X.; Nai, Z.G.; Liang, J.; Cao, B.C. Comparison of corrosion resistance and cytocompatibility of MgO and ZrO_2 coatings on AZ31 magnesium alloy formed via plasma electrolytic oxidation. *Coatings* **2018**, *8*, 441. [CrossRef]
22. Al-Radha, A.S.D.; Dymock, D.; Younes, C.; O'Sullivan, D. Surface properties of titanium and zirconia dental implant materials and their effect on bacterial adhesion. *J. Dent.* **2012**, *40*, 146–153. [CrossRef] [PubMed]
23. Liu, X.Y.; Huang, A.P.; Ding, C.X.; Chu, P.K. Bioactivity and cytocompatibility of zirconia (ZrO_2) films fabricated by cathodic arc deposition. *Biomaterials* **2006**, *27*, 3904–3911. [CrossRef] [PubMed]
24. Qin, H.; Zhao, Y.C.; An, Z.Q.; Cheng, M.Q.; Wang, Q.; Cheng, T.; Wang, Q.J.; Wang, J.X.; Jiang, Y.; Zhang, X.L.; et al. Enhanced antibacterial properties, biocompatibility, and corrosion resistance of degradable Mg–Nd–Zr alloy. *Biomaterials* **2015**, *53*, 211–220. [CrossRef] [PubMed]
25. Zhao, Y.; Jamesh, M.I.; Li, W.K.; Wu, G.S.; Wang, C.X.; Zheng, Y.F.; Yeung, K.W.K.; Chu, P.K. Enhanced antimicrobial properties, cytocompatibility, and corrosion resistance of plasma-modified biodegradable magnesium alloys. *Acta Biomater.* **2014**, *10*, 544–556. [CrossRef]
26. Kazanski, B.; Kossenko, A.; Zinigrad, M.; Lugovskoy, A. Fluoride ions as modifiers of the oxide layer produced by plasma electrolytic oxidation on AZ91D magnesium alloy. *Appl. Surf. Sci.* **2013**, *287*, 461–466. [CrossRef]
27. Chen, H.; Lv, G.H.; Zhang, G.L.; Pang, H.; Wang, X.Q.; Lee, H.J.; Yang, S.Z. Corrosion performance of plasma electrolytic oxidation oxidized AZ31 magnesium alloy in silicate solutions with different additives. *Surf. Coat. Technol.* **2010**, *205*, S32–S35. [CrossRef]
28. Yang, L.; Perez-Amodio, S.; Barrère-de Groot, F.Y.; Everts, V.; van Blitterswijk, C.A.; Habibovic, P. The effects of inorganic additives to calcium phosphate on in vitro behavior of osteoblasts and osteoclasts. *Biomaterials* **2010**, *31*, 2976–2989. [CrossRef]
29. Liu, H.Y.; Wang, X.J.; Wang, L.P.; Lei, F.Y.; Wang, X.F.; Ai, H.L. Effect of fluoride-ion implantation on the biocompatibility of titanium for dental applications. *Appl. Surf. Sci.* **2008**, *254*, 6305–6312. [CrossRef]
30. Habibovic, P.; Barralet, J.E. Bioinorganics and biomaterials: Bone repair. *Acta Biomater.* **2011**, *7*, 3013–3026. [CrossRef]
31. Zaze, A.C.S.F.; Dias, A.P.; Amaral, J.G.; Miyasaki, M.L.; Sassaki, K.T.; Delbem, A.C.B. In situ evaluation of low-fluoride toothpastes associated to calcium glycerophosphate on enamel remineralization. *J. Dent.* **2014**, *42*, 1621–1625. [CrossRef] [PubMed]
32. Pan, Y.K.; Chen, C.Z.; Wang, D.G.; Zhao, T.G. Effects of phosphates on microstructure and bioactivity of micro-arc oxidized calcium phosphate coatings on Mg–Zn–Zr magnesium alloy. *Colloids Surf. B.* **2013**, *109*, 1–9. [CrossRef] [PubMed]
33. Hu, R.; Su, Y.Y.; Liu, H.D.; Cheng, J.; Yang, X.; Shao, Z.C. The effect of adding corrosion inhibitors into an electrolyte nickel plating bath for magnesium alloys. *J. Mater. Eng. Perform.* **2016**, *25*, 4530–4536. [CrossRef]
34. Hu, R.; Su, Y.Y.; Liu, H.D. Deposition behaviour of nickel phosphorus coating on magnesium alloy in a weak corrosive electroless nickel plating bath. *J. Alloy. Compd.* **2016**, *658*, 555–560. [CrossRef]
35. Dou, J.H.; Wang, C.Y.; Gu, G.C.; Chen, C. Formation of silicon-calcium-phosphate-containing coating on Mg–Zn–Ca alloy by two-step micro-arc oxidation technique. *Mater. Lett.* **2018**, *212*, 37–40. [CrossRef]
36. Ma, Y.; Nie, X.; Northwood, D.O.; Hu, H. Systematic study of the electrolytic plasma oxidation process on a Mg alloy for corrosion protection. *Thin Solid Films* **2006**, *494*, 296–301. [CrossRef]
37. Zhu, X.L.; Chen, J.; Scheideler, L.; Reichl, R.; Geis-Gerstorfer, J. Effects of topography and composition of titanium surface oxides on osteoblast responses. *Biomaterials* **2004**, *25*, 4087–4103. [CrossRef]

38. Guo, S.F.; Zhang, H.J.; Liu, Z.; Chen, W.; Xie, S.F. Corrosion resistance of amorphous and crystalline Zr-based alloys in simulated seawater. *Electrochem. Commun.* **2012**, *24*, 39–42. [CrossRef]
39. Lee, K.M.; Shin, K.R.; Namgung, S.; Yoo, B.; Shin, D.H. Electrochemical response of ZrO_2-incorproated oxide layer on AZ91 Mg alloy processed by plasma electrolytic oxidation. *Surf. Coat. Technol.* **2011**, *205*, 3779–3784. [CrossRef]
40. Zhang, R.Y.; Cai, S.; Xu, G.H.; Zhao, H.; Li, Y.; Wang, X.X.; Huang, K.; Ren, M.G.; Wu, X.D. Crack self-healing of phytic acid conversion coating on AZ31 magnesium alloy by heat treatment and the corrosion resistance. *Appl. Surf. Sci.* **2014**, *313*, 896–904. [CrossRef]
41. Zeng, Y.F.; Ko, T.P.; Lai, H.L.; Cheng, Y.S.; Wu, T.H.; Ma, W.H.; Chen, C.C.; Yang, C.S.; Cheng, K.J.; Huang, C.H.; et al. Crystal structures of bacillus alkaline phytase in complex with divalent metal ions and inositol hexasulfate. *J. Mol. Biol.* **2011**, *409*, 214–224. [CrossRef] [PubMed]
42. Sun, T.; Ning, W.M.; Yu, Y.Q.; Zhang, G.R. Appendix 3: Solubility product constants at 298.15 K. In *University Chemistry (I)*; Ning, W.M., Ed.; Northeast University Press: Shenyang, China, 1993; p. 402. (In Chinese)
43. Rehaman, Z.U.; Shin, S.H.; Hussain, I.; Koo, B.H. Investigation of hybrid PEO coatings on AZ31B magnesium alloy in alkaline K_2ZrF_6–Na_2SiO_3 electrolyte solution. *Prot. Met. Phys. Chem.* **2017**, *53*, 495–502. [CrossRef]
44. An, L.Y.; Ma, Y.; Liu, Y.P.; Sun, L.; Wang, S.; Wang, Z.Y. Effects of additives, voltage and their interactions on PEO coatings formed on magnesium alloys. *Surf. Coat. Technol.* **2018**, *354*, 226–235. [CrossRef]
45. Apelfeld, A.; Krit, B.; Ludin, V.; Morozova, N.; Vladimirov, B.; Wu, R.Z. The characteristics of plasma electrolytic oxidation coatings on AZ41 magnesium alloy. *Surf. Coat. Technol.* **2017**, *322*, 127–133. [CrossRef]
46. Mohedano, M.; Arrabal, R.; Mingo, B.; Pardo, A.; Matykina, E. Role of particle type and concentration on characteristics of PEO coatings on AM50 magnesium alloy. *Surf. Coat. Technol.* **2018**, *334*, 328–335. [CrossRef]
47. Notoya, T.; Otieno-Alego, V.; Schweinsberg, D.P. The corrosion and polarization behaviour of copper in domestic water in the presence of Ca, Mg, and Na-salts of phytic acid. *Corros. Sci.* **1995**, *37*, 55–65. [CrossRef]
48. Guo, X.L.; Feng, Z.C. Belinda Hurley, Rudolph Buchheit, Entrapped molybdate in phytate film and the corresponding anodic corrosion inhibition on AA2024-T3. *J. Electrochem. Soc.* **2016**, *163*, C260–C268. [CrossRef]
49. Yi, A.H.; Du, J.; Wang, J.; Mu, S.L.; Zhang, G.Z.; Li, W.F. Preparation and characterization of colored Ti/Zr conversion coating on AZ91D magnesium alloy. *Surf. Coat. Technol.* **2015**, *276*, 239–247. [CrossRef]

© 2019 by the authors. Licensee MDPI, Basel, Switzerland. This article is an open access article distributed under the terms and conditions of the Creative Commons Attribution (CC BY) license (http://creativecommons.org/licenses/by/4.0/).